N90-22656

Program 4 Measurements and Mechanisms of Localized Aqueous Corrosion in Aluminum-Lithium Alloys

Rudolph G. Buchheit, Jr. and Glenn E. Stoner

Objectives

The objective of this research is to characterize the localized corrosion and stress corrosion crack initiation behavior of Al-Li-Cu alloy 2090, and to gain an understanding of the role of local corrosion and occluded cell environments in the mechanisms of pitting and initiation and early-stage propagation of stress corrosion cracks.

Stress Corrosion in 2090: The Role of Localized Corrosion in the Subgrain Boundary Region

R. G. Buchheit
G. E. Stoner

Department of Materials Science

Like most heat treatable aluminum alloys, localized corrosion and stress corrosion of Al-Li-Cu alloys is strongly dependent on the nature and distribution of second phase particles. To develop a mechanistic understanding of the role of localized corrosion in the stress corrosion process, bulk samples of T_1 (Al_2CuLi) and a range of Al-Cu-Fe impurity phases were prepared for electrochemical experiments. Potentiodynamic polarization and galvanic couple experiments were performed in standard 0.6 M NaCl and in simulated crevice solutions to assess corrosion behavior of these particles with respect to the α-Al matrix.

A comparison of time to failure versus applied potential using a constant load, smooth bar SCC test technique in Cl^-, Cl^-/CrO_4^{2-} and Cl^-/CO_3^{2-} environments shows that rapid failures are to be expected when applied potentials are more positive than the breakaway potential (E_{br}) of T_1 (crack tip) but less than E_{br} of α-Al (crack walls). It is shown that this criterion is not satisfied in aerated Cl^- solutions. Accordingly, SCC resistance is good. This criterion is satisfied, however, in an alkaline isolated fissure exposed to a CO_2 containing atmosphere. Rapid failure induced by these fissures has recently been termed "preexposure embrittlement."

Anodic polarization shows that the corrosion behavior of T_1 is relatively unaffected in alkaline CO_3^{2-} environments but the α-Al phase is rapidly passivated. X-ray diffraction of crevice walls from artificial crevices suggests that passivation of α-Al occurs as Bayerite ($Al(OH)_3$) imbibes solvated lithium and carbonate ions to form a hydrotalcite-type compound $[LiAl_2(OH)_6]_2^+ \cdot CO_3^{2-} \cdot nH_2O$.

Stress Corrosion of 2090: The Role of Localized Corrosion in the Subgrain Boundary Region

R.G. Buchheit
G.E. Stoner

Department of Materials Science
University of Virginia
Charlottesville, Virginia 22901

Sponsored by NASA, Langley Research Center, Hampton, Virginia

Outline

* Microstructural Heterogeneity and Localized Corrosion

* Time to Failure vs. Applied Potential in Cl^- and Cl^-/CrO_4^{2-}

* SCC in CO_3^{2-} Environments, "Pre-Exposure Embrittlement"

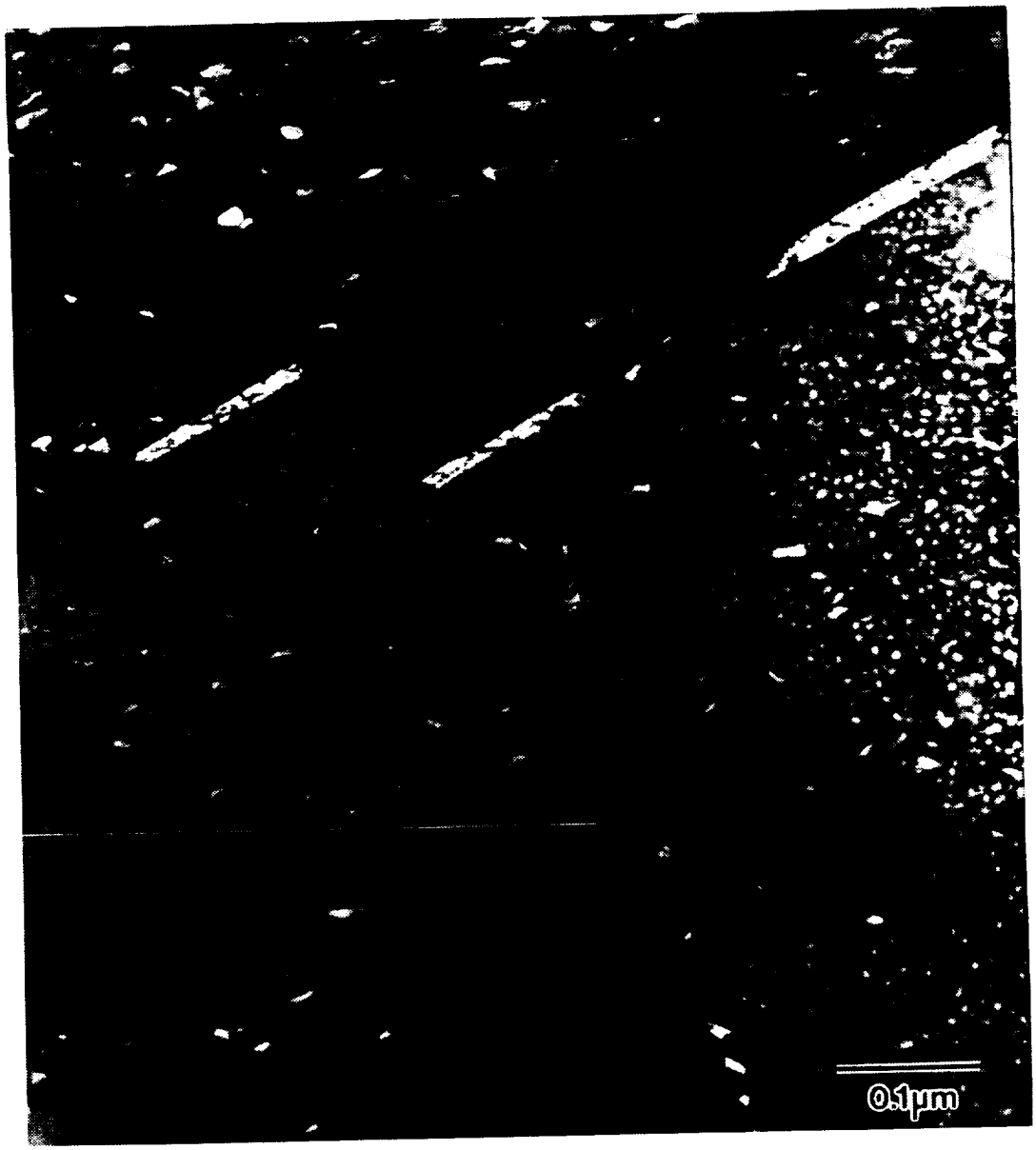

Centered dark field transmission electron micrograph of the subgrain boundary region showing the precipitation of T_1 on boundaries and in subgrains.

Corrosion Behavior in Aerated 0.6 M NaCl

Phase	Model Material	Corrosion Potential (mV_{sce})	Galvanic Couple Current Density (ua/cm^2)
α - Al	SHT 2090	-720	----
Al-14Cu	as cast	-620	-0.5
Al18-Cu-5Fe	as cast	-670	-7.0
Al-24Cu-5Fe	as cast	-675	-3.0
T_1	Al-26Cu-21Li	-1100	+500
PA 2090	Al-3Cu-2Li	-720	----

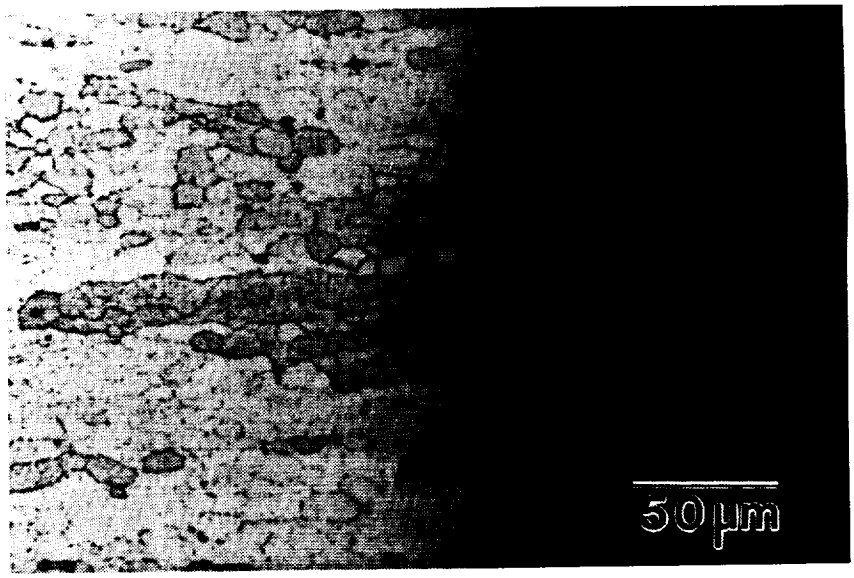

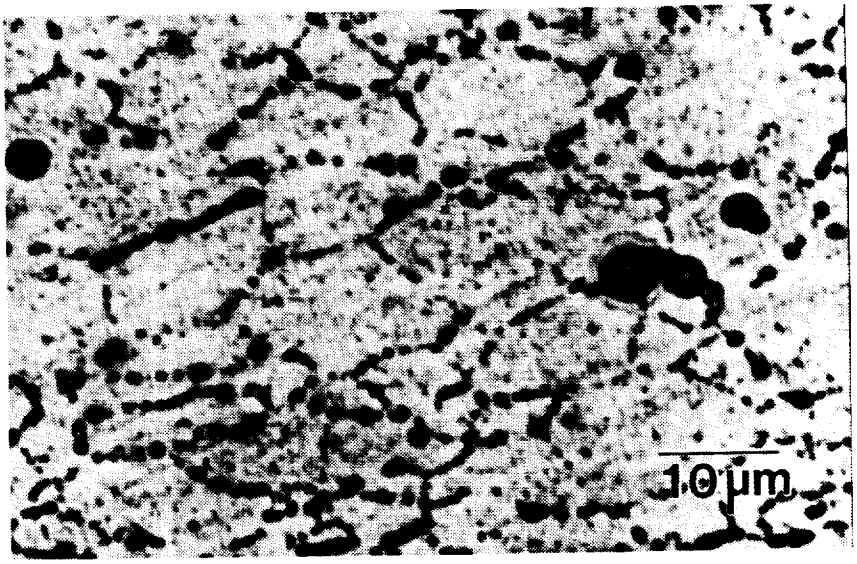

A. Optical micrograph of pitting associated with Al-Fe-Cu impurity particles.

B. Optical micrograph of discontinuous subgrain boundary pitting associated with T_1 precipitated on subgrain boundaries.

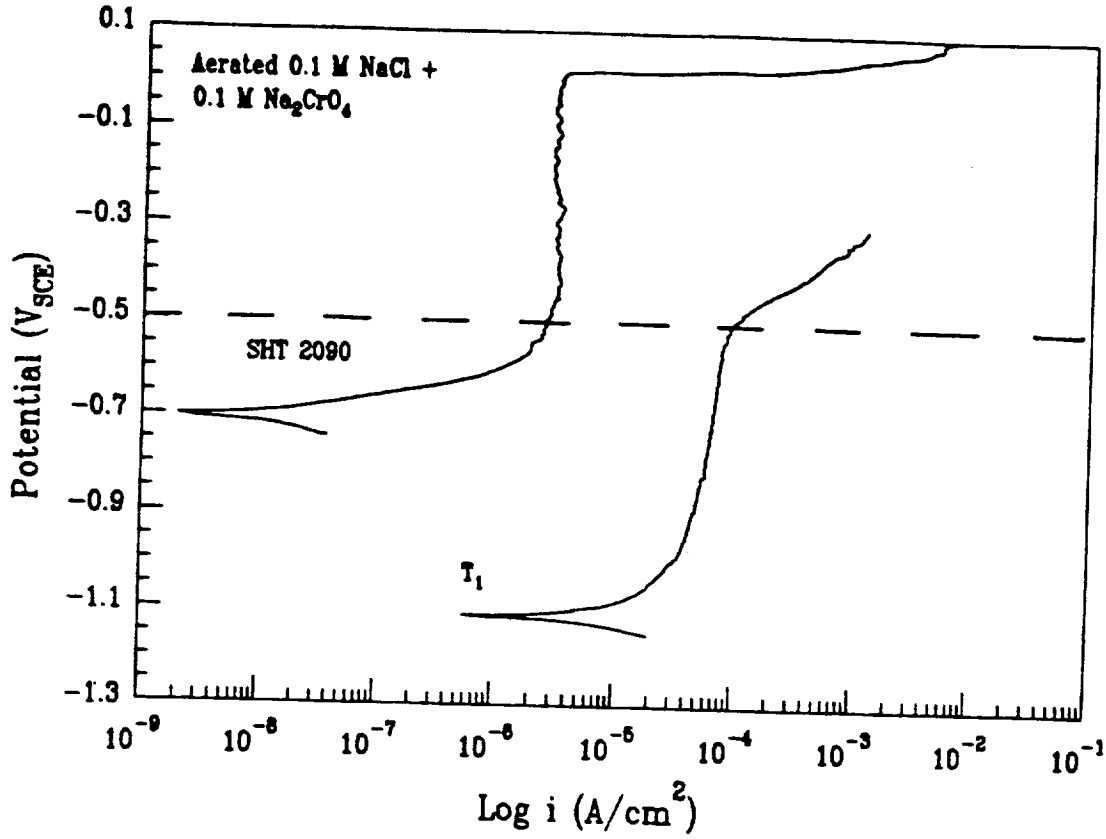

Anodic polarization in Cl^-/CrO_4^{2-}

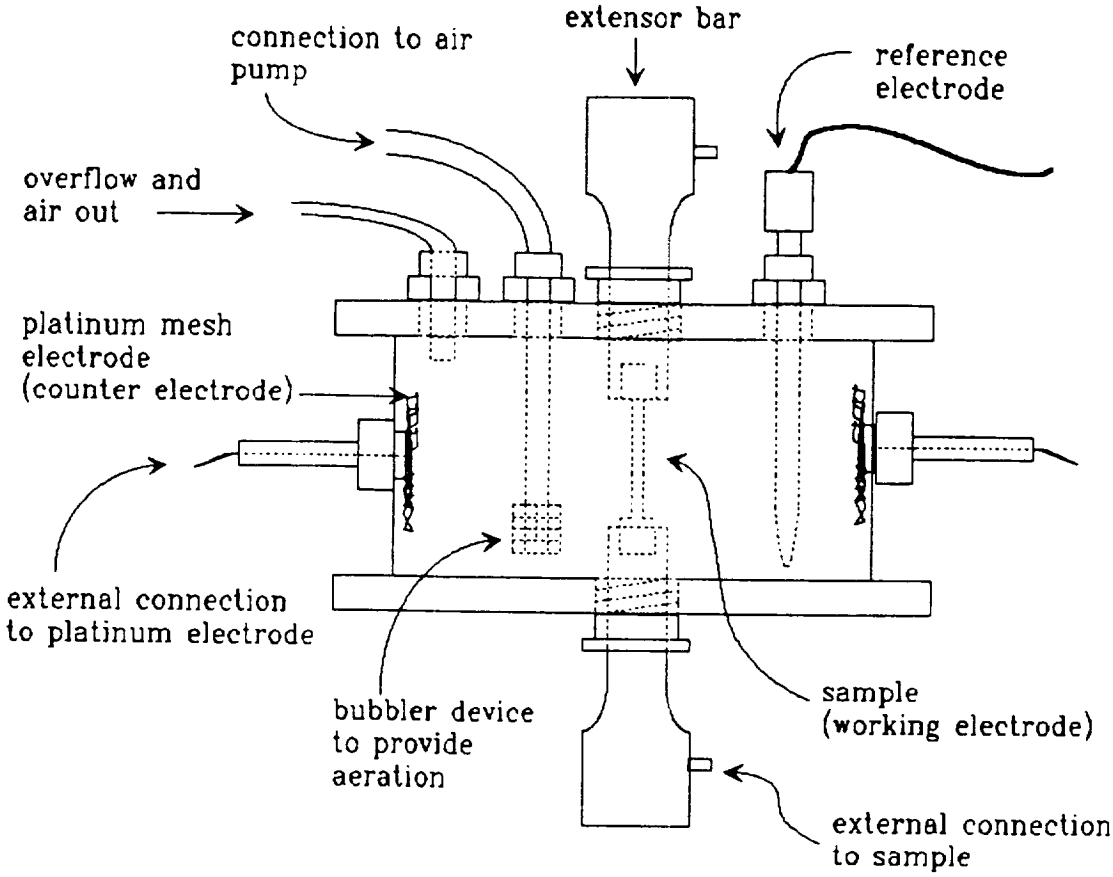

Schematic of the cell used for constant load TTF experiments.

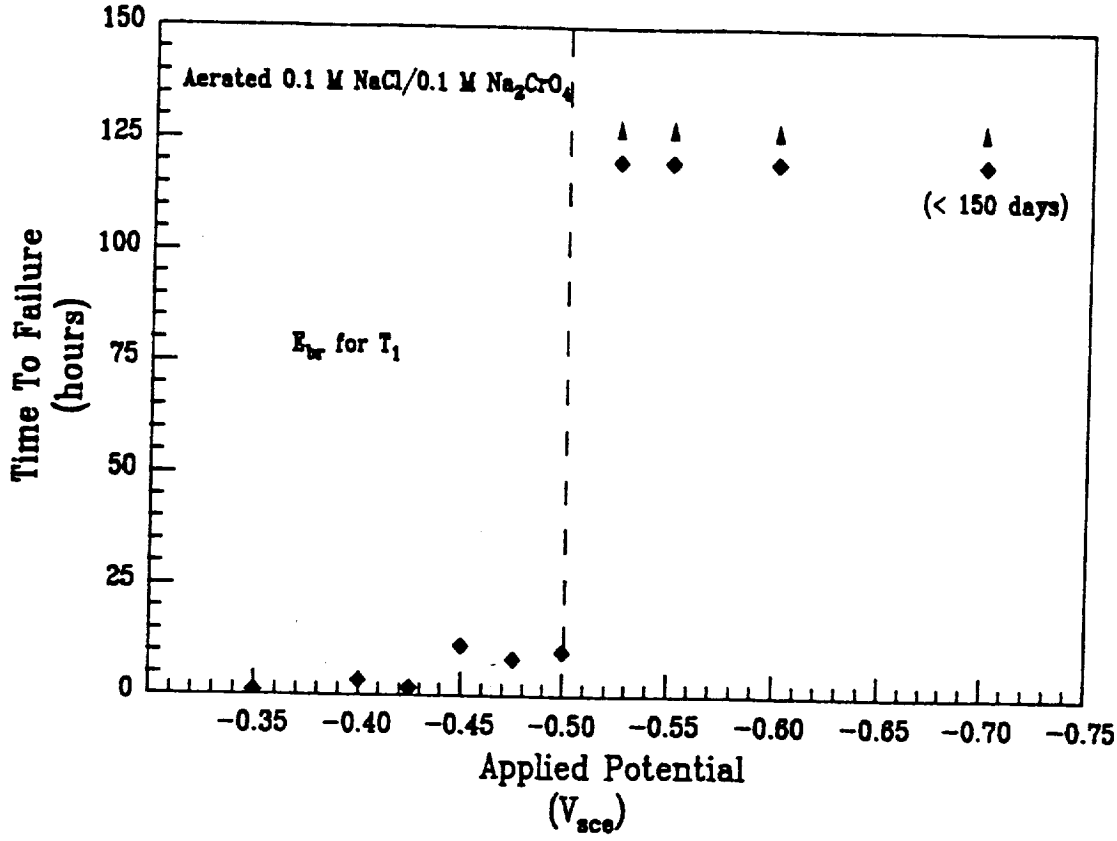

Time to failure versus applied potential in Cl^-/CrO_4^{2-}

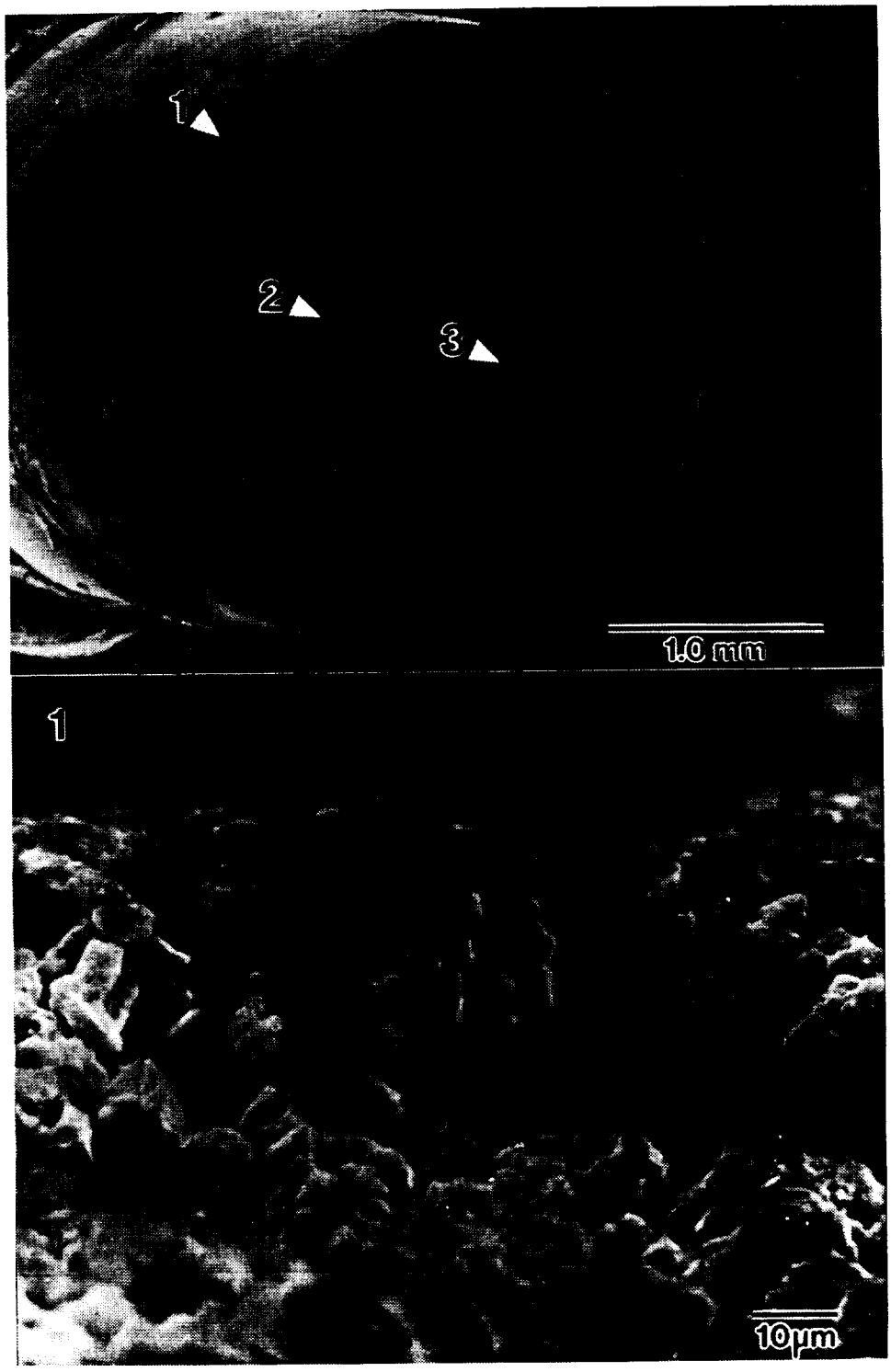

A. Scanning electron micrograph of the fracture surface of a 2090 tensile specimen subjected to a time to failure experiment at 55 % of the S-T yield strength in 0.1 M NaCl + 0.1 M Na_2CrO_4 at an applied potential greater than E_{br} of T_1.

B. Scanning electron micrograph from the rim of the failure initiating pit.

C. Scanning electron micrograph of the SCC propagation region 200 micrometers below the base of the pit.

D. Scanning electron micrograph of the tensile overload region.

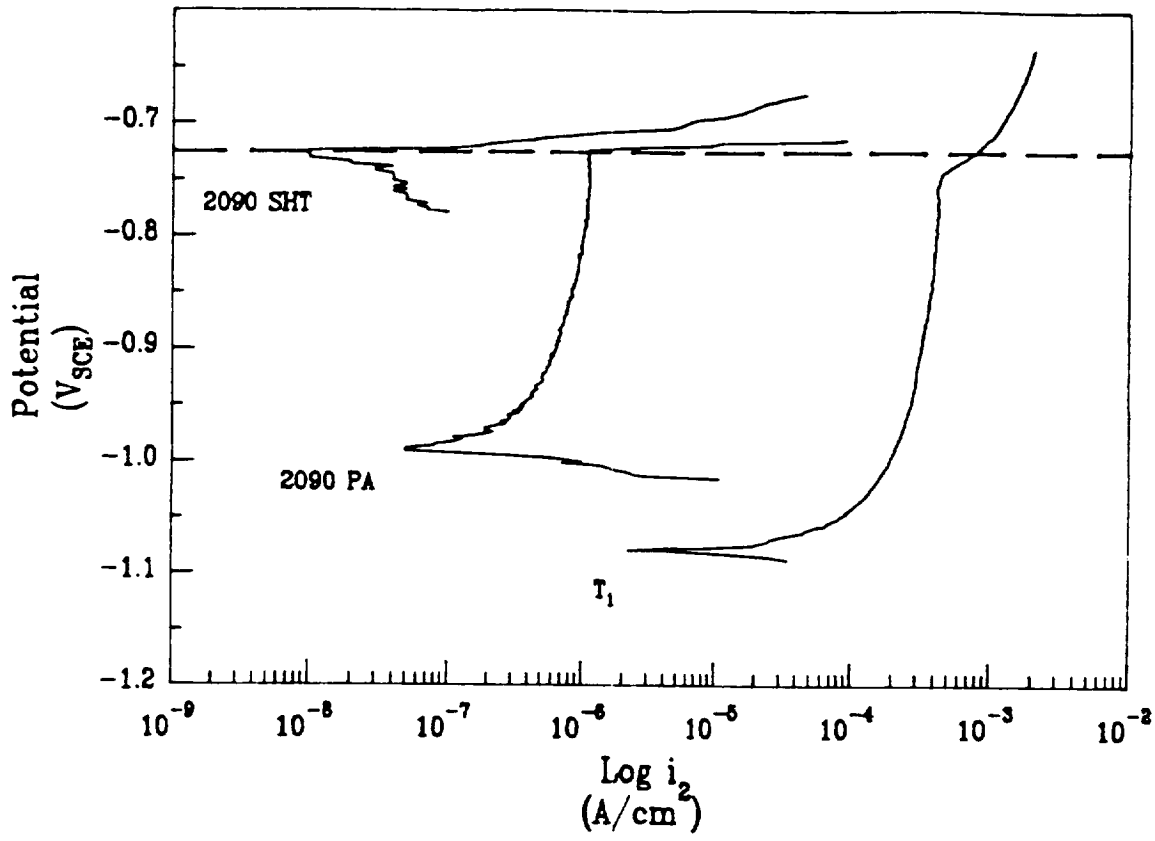

Anodic polarization in 0.6 M NaCl solution

Time to Failure vs. Applied Potential
in Aerated 0.6 M NaCl

Applied Potential (mV_{sce})	Time to Failure (days)
-720 (E_{corr})	3 @ > 75 5 @ > 30
-715	2 @ > 45
-1150	2 @ > 45

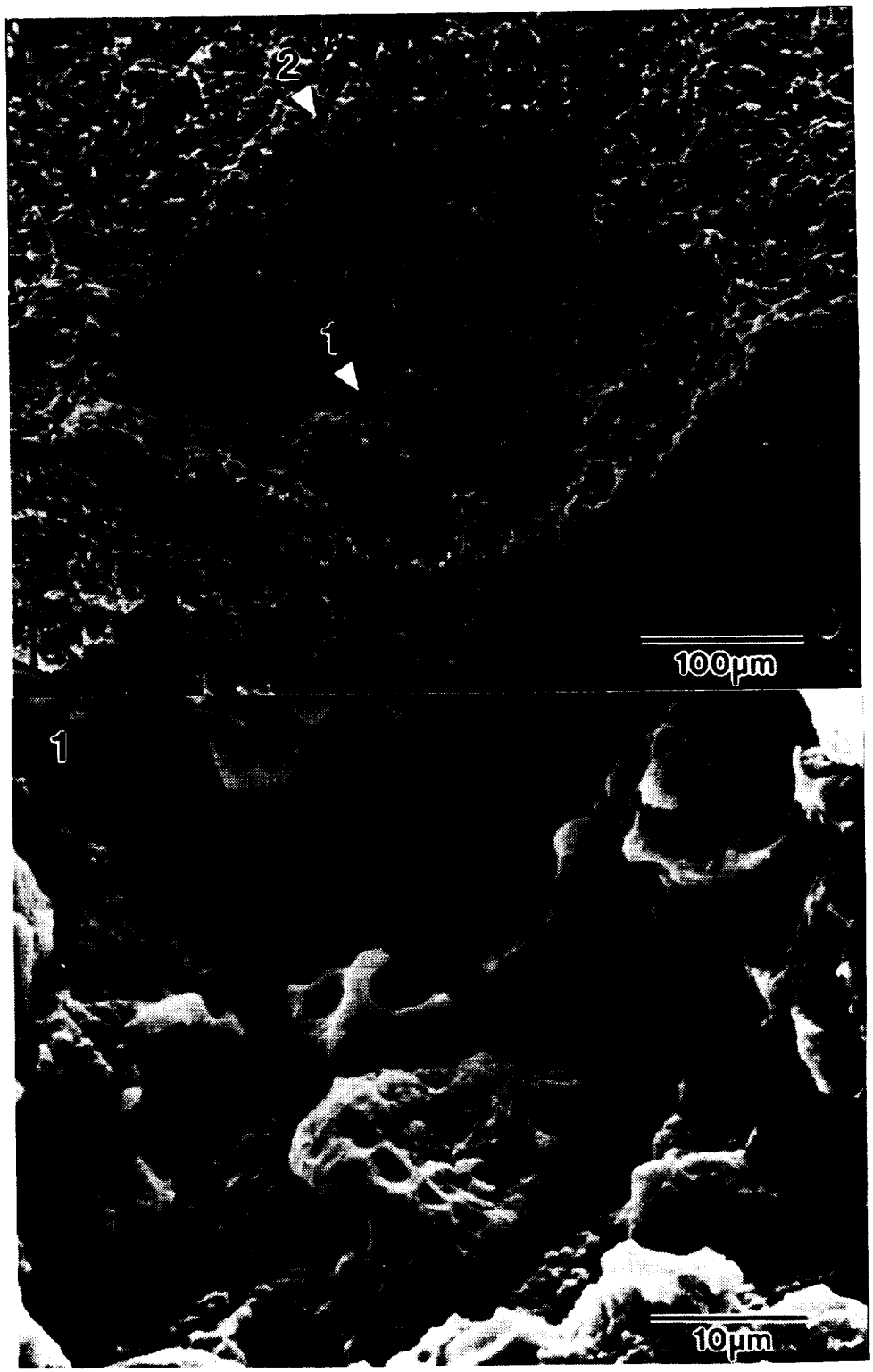

A. Scanning electron micrograph of the fracture surface of a 2090 specimen loaded to 55% of the S-T yield and immersed in 0.6 M NaCl solution under free corrosion conditions for 7 days then removed from solution and pulled to fracture in air.

B. Scanning electron micrograph of the failure initiating pit.

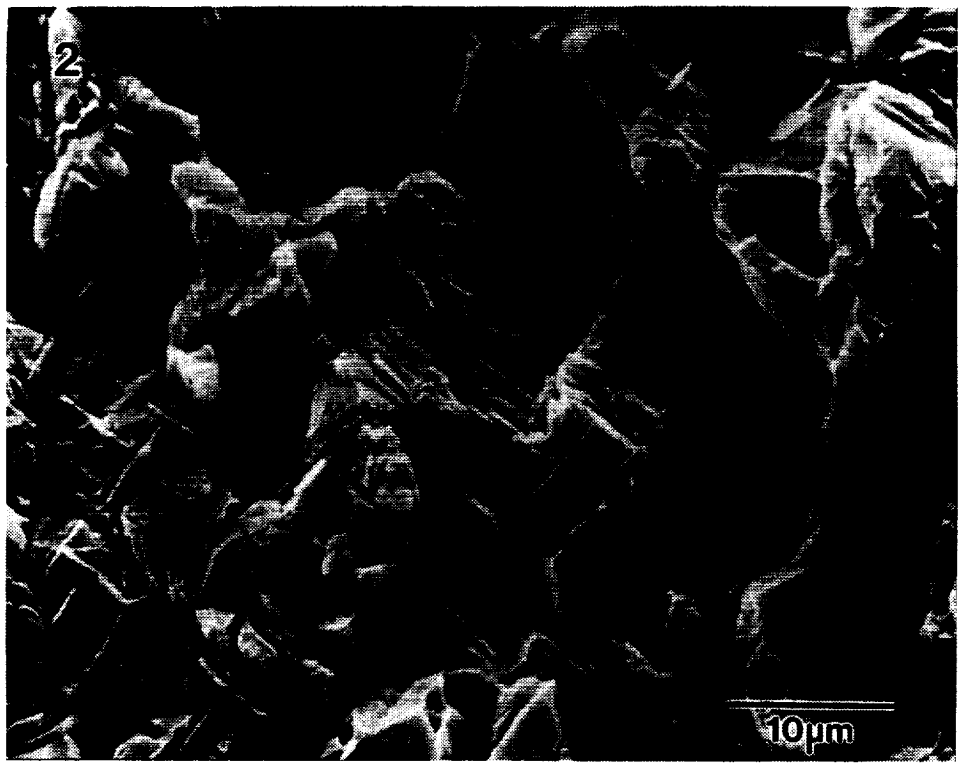

C. Scanning electron micrograph of the overload region directly below the base of the pit.

Necessary Conditions for Rapid SCC Failure Appear to be:

* α - Al passive (below E_{br})

* T_1 transpassive (above E_{br})

Pre-Exposure Embrittlement

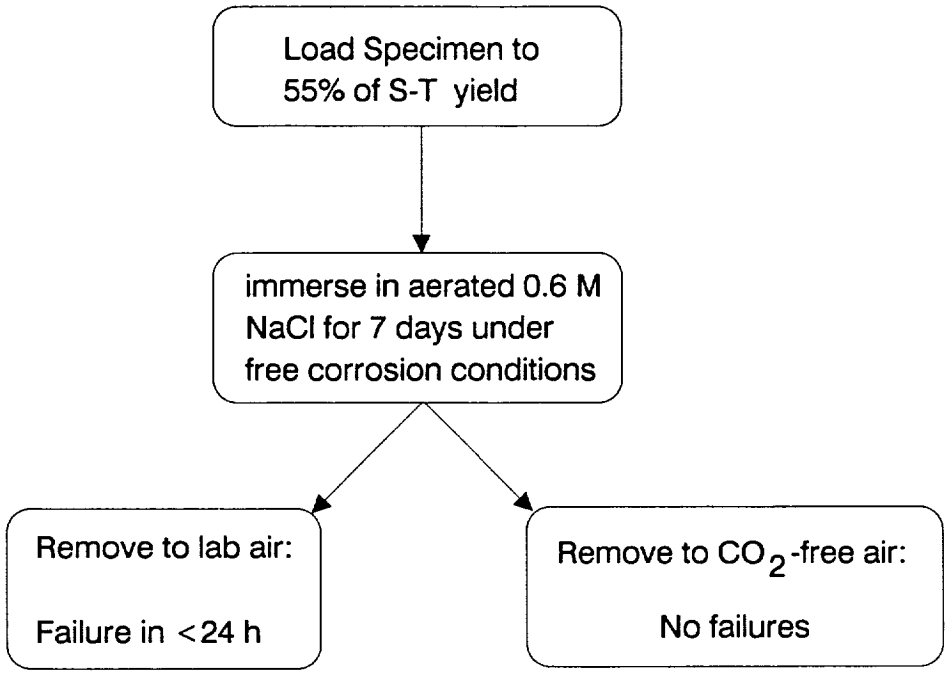

* Alloy 8090, Holroyd, et al. (1987)

* Alloy 2090, Moran (1989)

Holroyd, et al.

Aerated 0.6 M NaCl too aggressive towards subgrain boundaries

Fissures become alkaline

Absorption of CO_2
pH falls
$LiAlO_2$ precipitates

SCC initiates and propagates

Moran

Continuous SGB corrosion in pits

Remove from solution

Li^+ and CO_3^{2-} upon removal

Li_2CO_3 precipitates
@ pH 10
$[CO_3^{2-}] = 1.0$ M
$[Li^+] = 0.144$ M reqd.

SCC initiates and propagates

Corrosion Behavior in Cl^- and Cl^-/CO_3^{2-}

	phase	i_{pass} (ua/cm^2)	E_{br} (mV_{sce})
0.6 M NaCl pH = 7 - 8	α - Al	1.0	-690
	T_1	200	-720
0.6 M NaCl + 0.1 M Li_2CO_3 pH = 10	α - Al	0.75	-590
	T_1	550	-720

-590 mV > Rapid Failure Window > -720 mV

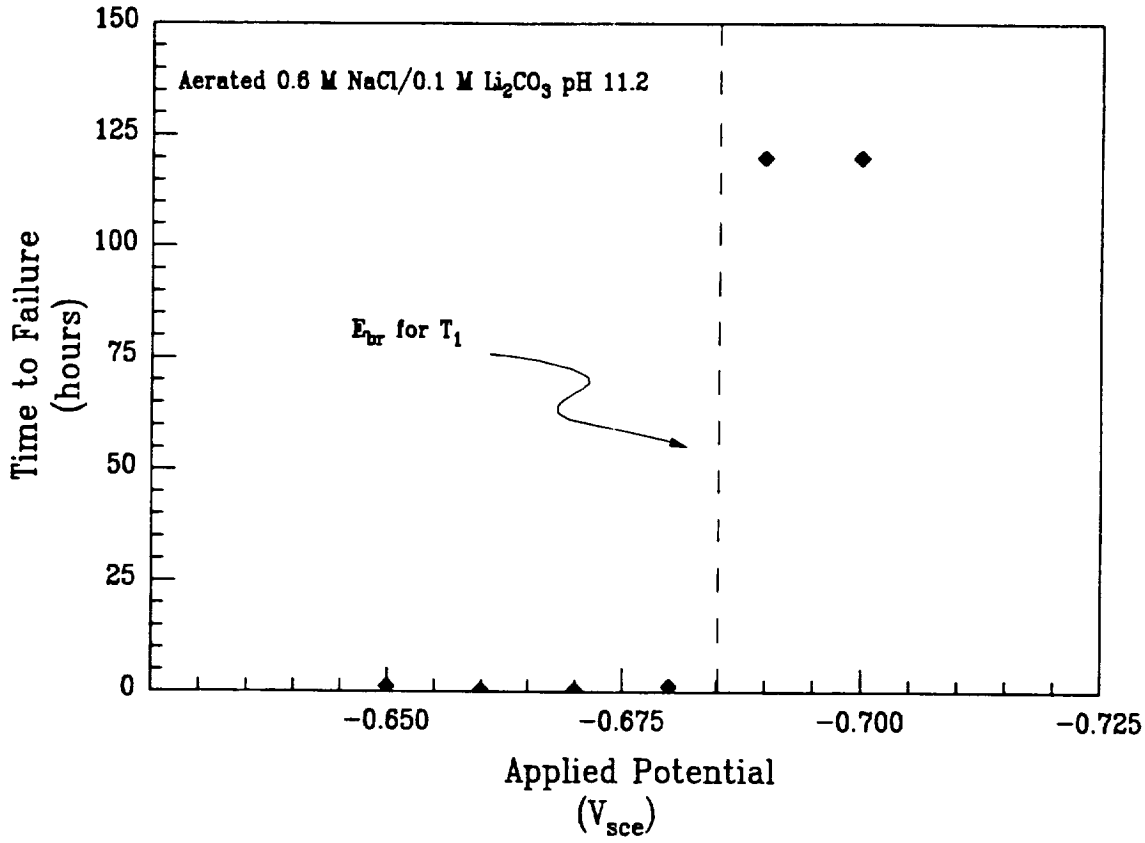

Time to failure versus applied potential in Cl^-/CO_3^{2-}

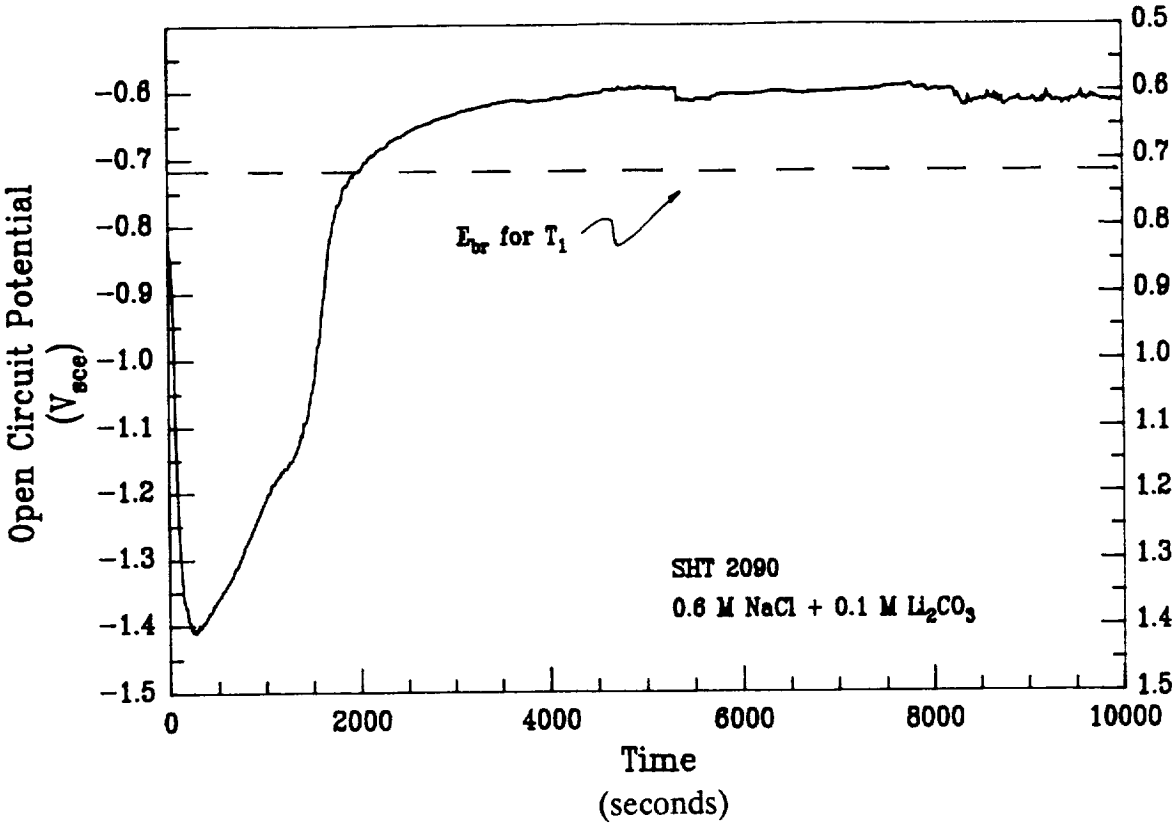

Open circuit potential versus time in Cl^-/CO_3^{2-}

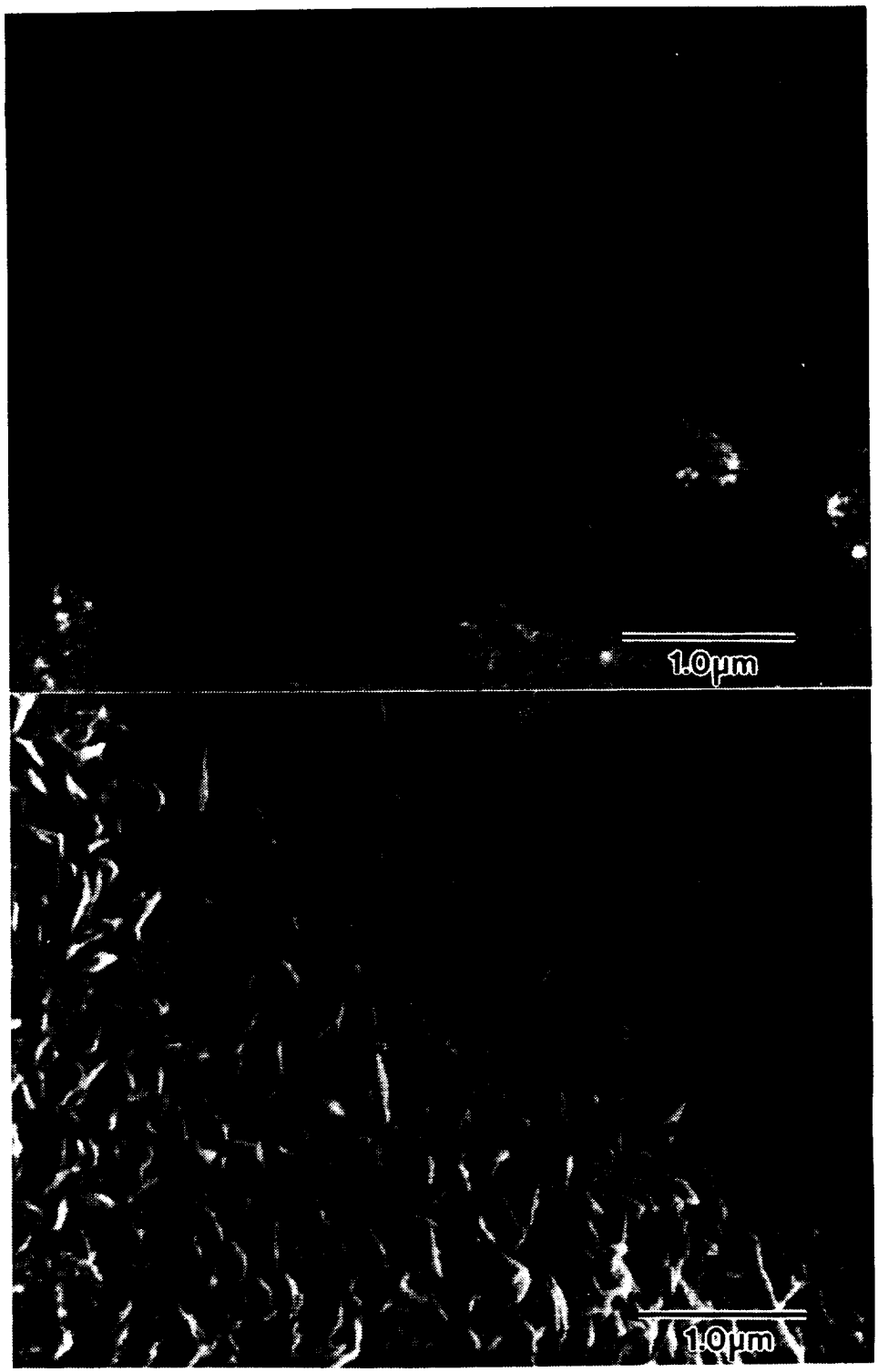

A. Scanning electron micrograph of the film that forms in the SCC region of a 2090 tensile specimen where the specimen is immersed in aerated 0.6 M NaCl for 7 days then removed to CO_2-free air.

B. Scanning electron micrograph of the film that forms in the SCC region of a 2090 tensile specimen that is immersed in aerated 0.6 M NaCl for 7 days then removed to laboratory air.

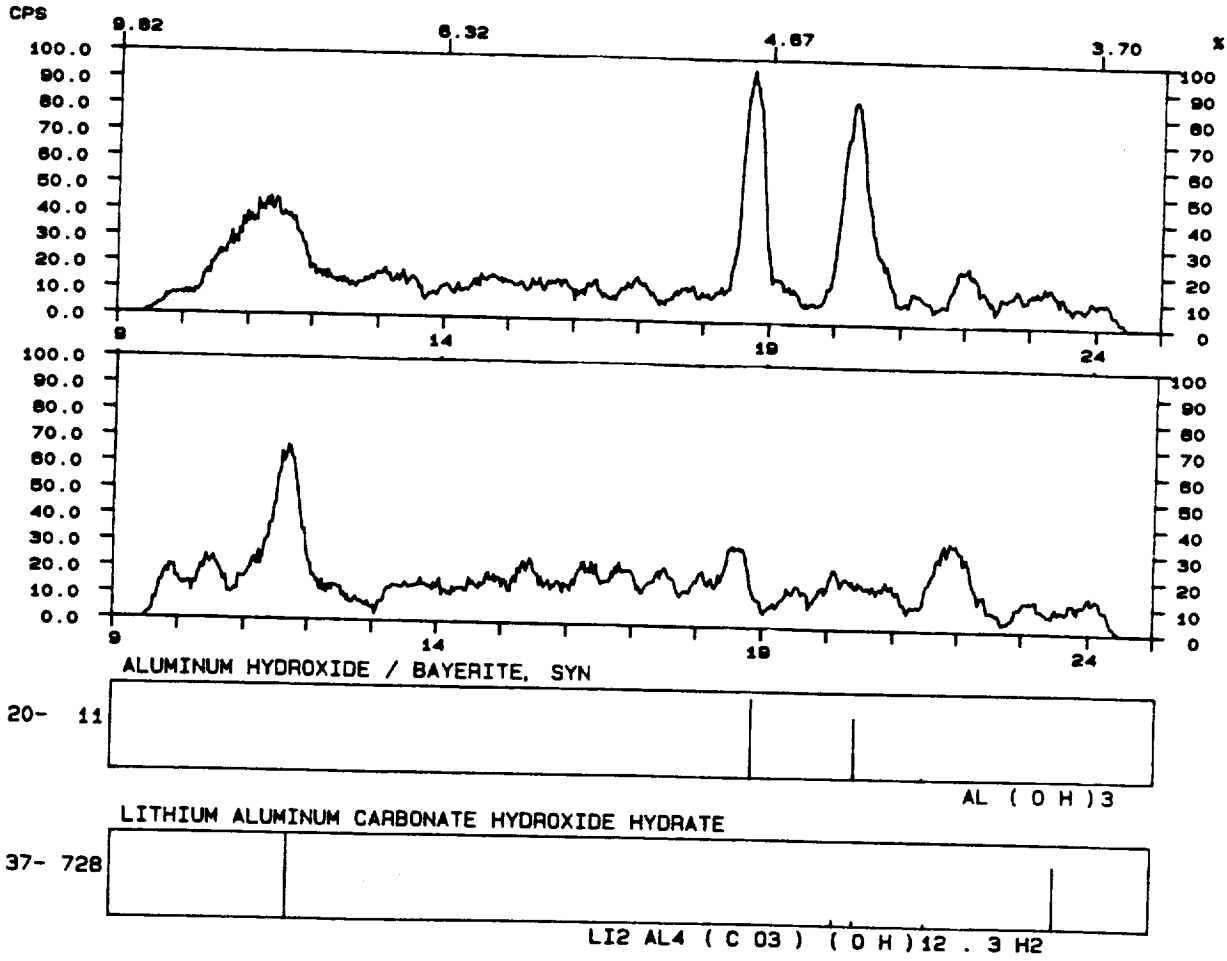

* hydrotalcite -type compound $[LiAl_2(OH)_6]^{+}_2 \cdot CO^{2-}_3 \cdot nH_2O$

* derived from bayerite $Al(OH)_3$

Hydrotalcites

* Alumina Gels + Lithium Salts $\longrightarrow$ $(LiX_x)_y \cdot 2(AlOH)_3 \cdot nH_2O$

* Several anions produce isomorphous compounds

OH^- Cl^-

* Passivating effects associated with its presence (Perrota, 1990)

* Insoluble in alkaline solutions

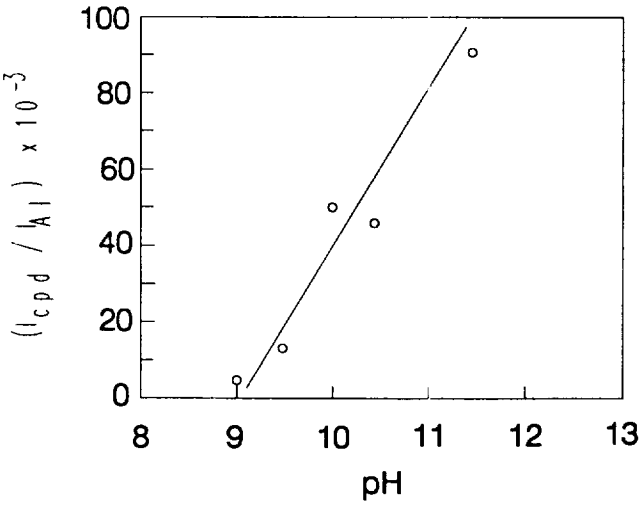

Ammended Pre-Exposure Embrittlement Mechanism

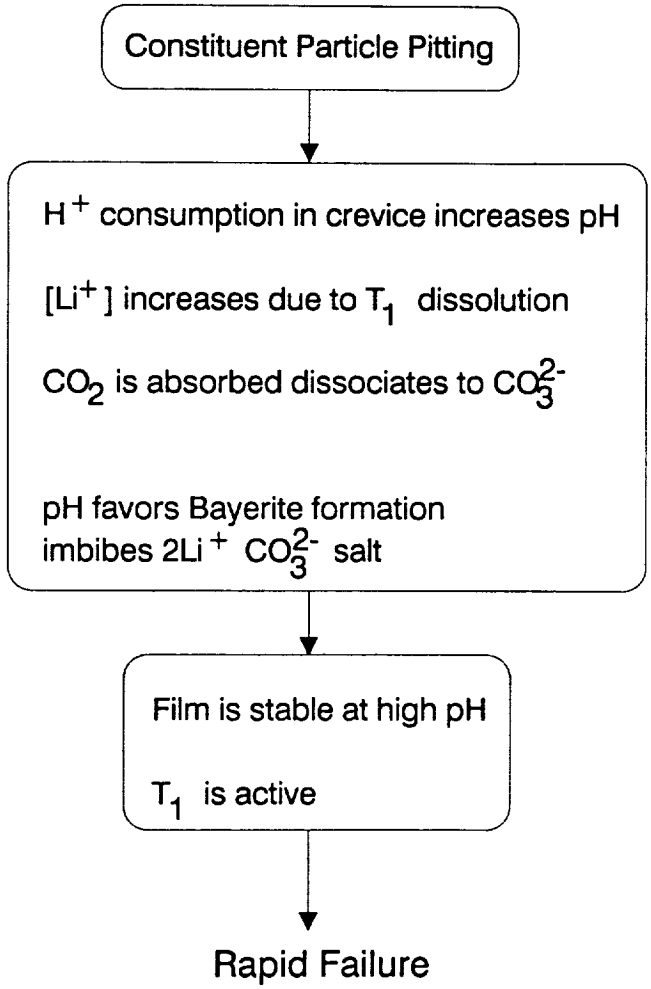

Summary

* In order of increasing nobility:
  T_1 < α - Al < Al-Cu-Fe

* Rapid SCC ensues when:
  $E_{br}T_1$ > $E_{applied}$ > $E_{br}\alpha$ - Al

* In 0.6 M NaCl, $E_{br}T_1$ = $E_{br}\alpha$ - Al
  rapid SCC criterion is not satified

* In isolated fissures, rapid SCC criterion is satisfied

* α - Al is passivated by a hydrotalcite-type compound

The following pages are from a presentation given at the CORROSION/90 Meeting, April 23-27, Las Vegas, Nevada

The Role of Hydrolysis in Crevice Corrosion of Aluminum-Lithium-Copper Alloys

R.G. Buchheit
J.P. Moran
G.E. Stoner

Center for Electrochemical Sciences and Engineering
Department of Materials Science
University of Virginia
Charlottesville, VA 22903

Sponsored by NASA, Langley Research Center, Hampton, VA under Contract No. NAG-745-2, D.L. Dicus Contract Monitor.

Overview

* Background
* Objectives
* Approach
* Results
* Summary

Background

Crevice coupled to Bulk Solution

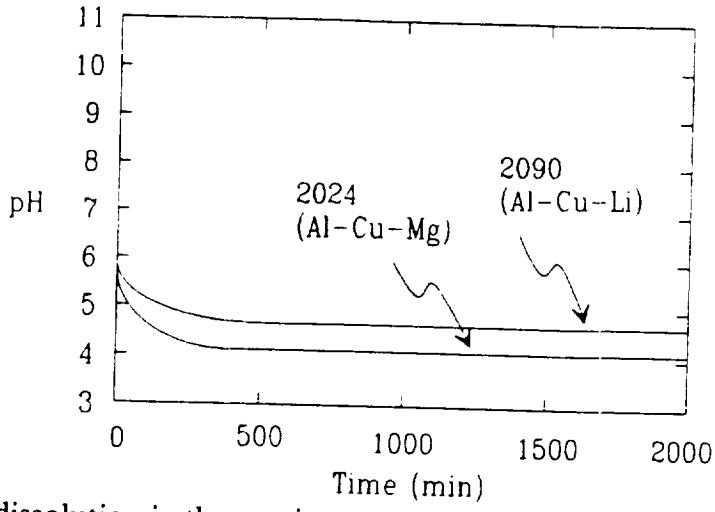

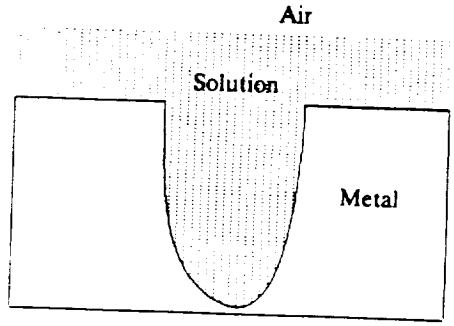

dissolution in the crevice

reduction reactions outside the crevice

Isolated Crevice

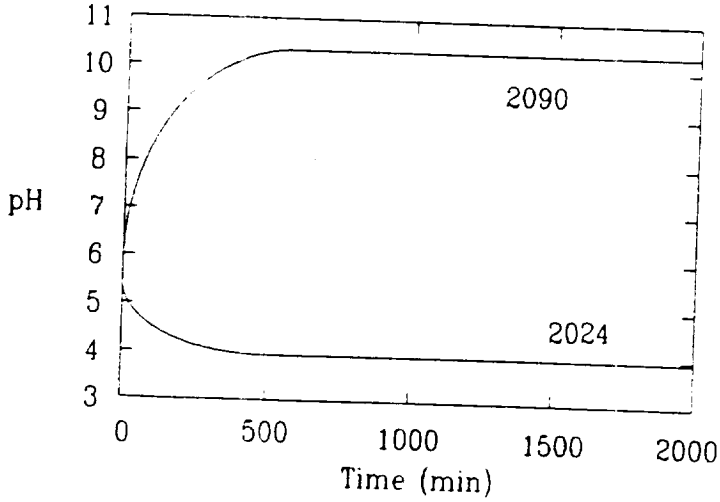

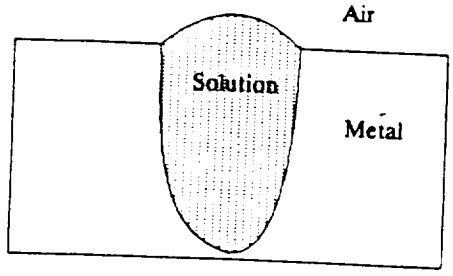

dissolution in the crevice

reduction reactions inside crevice

Objectives

Separate and identify the roles of:

- Al^{3+}
- Li^{+}
- Cu^{2+}

} hydrolysis

- an external cathode

Approach

Simulated crevice technique

* in situ measurement

* avoid the size constraint associated with real crevices

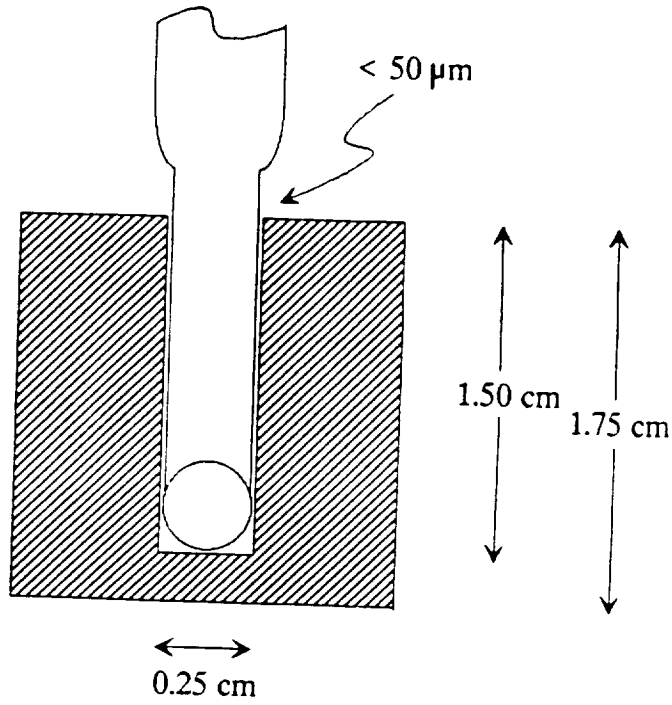

Measure pH versus Time for:

Materials

99.99 Al
SHT Al-3Li
SHT Al-3Cu
SHT Al-3Cu-2Li

Environments

Aerated Bulk Solution
Isolated Crevice

Approach

Interpret steady state pH using Distribution Diagrams for monomeric hydrolysis products and knowledge of where electrochemical reduction reactions are occurring.

Monomeric Hydrolysis

$$xM^{z+} + yH_2O \leftrightarrow M_x(OH)_y^{(xz-y)+} + yH^+$$

* Rapid $10^5 < k < 10^{10}$ moles^{-1}sec^{-1}
* Reversible
* An equilibrium treatment is applicable

Reactions Considered

	$-\log K_{xy}$
<u>Aluminum</u>	
$Al^{3+} + H_2O \leftrightarrow AlOH^{2+} + H^+$	4.97
$Al^{3+} + 2H_2O \leftrightarrow Al(OH)_2^+ + 2H^+$	9.3
$Al^{3+} + 3H_2O \leftrightarrow Al(OH)_3 + 3H^+$	15.0
$Al^{3+} + 4H_2O \leftrightarrow Al(OH)_4^- + 4H^+$	23.0
<u>Lithium</u>	
$Li^+ + H_2O \leftrightarrow LiOH + H^+$	13.86
<u>Copper</u>	
$Cu^{2+} + H_2O \leftrightarrow CuOH^+ + H^+$	8.0
$Cu^{2+} + 2H_2O \leftrightarrow Cu(OH)_2 + 2H^+$	17.3
$Cu^{2+} + 3H_2O \leftrightarrow Cu(OH)_3^- + 3H^+$	27.8
$Cu^{2+} + 4H_2O \leftrightarrow Cu(OH)_4^{2-} + 4H^+$	39.6
$Cu^{2+} + H_2O \leftrightarrow 1/2Cu_2(OH)_2^{2+} + H^+$	10.36
<u>Electrochemical Reactions</u>	
$M \rightarrow M^{n+} + ne^-$	internal
$O_2 + 4H^+ + 4e^- \rightarrow 2H_2O$	external
$2H^+ + 2e^- \rightarrow H_2$	internal
$H_2O + e^- \rightarrow H + OH^-$	internal

Construction of Distribution Diagrams

Formation Quotients (Baes and Mesmer, 1986.)

$$\log Q_{xy} = \log K_{xy} + \frac{aI^{1/2}}{(1 + I^{1/2})} + bI$$

$$I = \frac{\Sigma z_i^2[i]}{2}$$

Mass Action Expressions

$$Q_{11} = \frac{[AlOH^{2+}][H^+]}{[Al^{3+}]}$$

.
.
.

$$F_{AlOH^{2+}} = \frac{[AlOH^{2+}]}{\Sigma\,[species]}$$

Distribution Diagrams

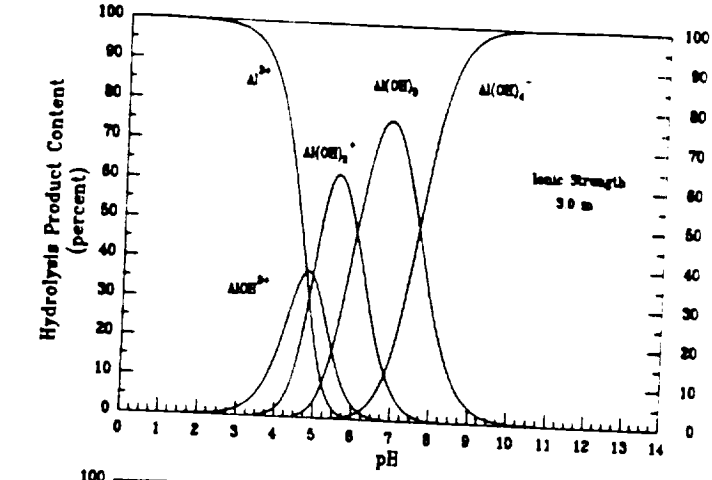

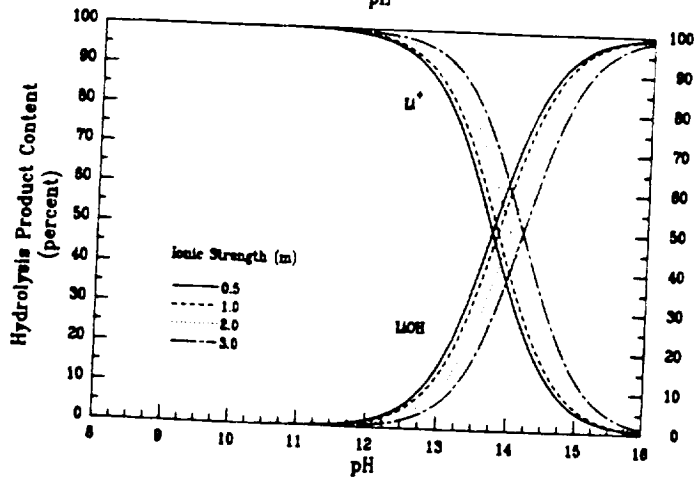

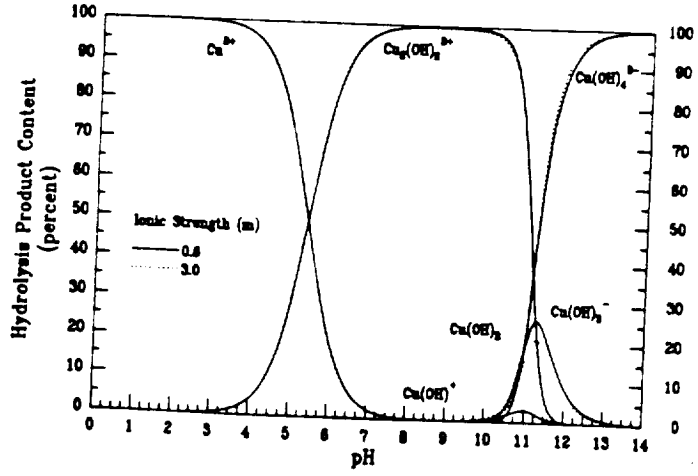

Results for Pure Aluminum

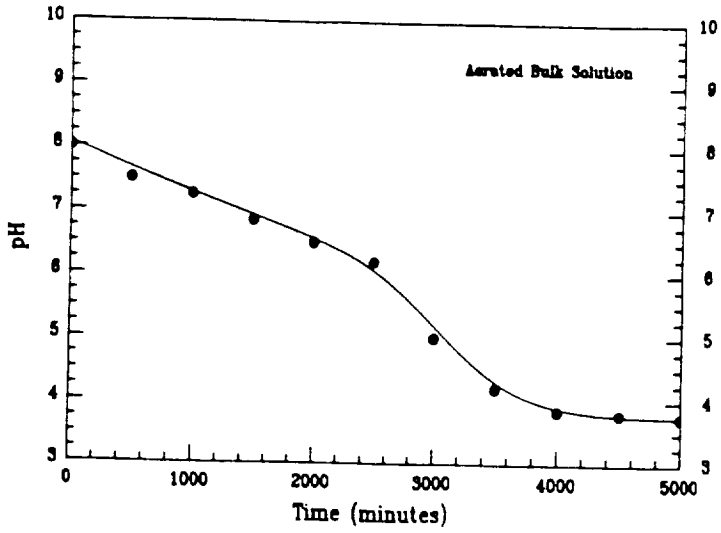

Electrochemical Reactions:

$Al \rightarrow Al^{3+} + 3e^-$ internal

$O_2 + 4H^+ + 4e^- \rightarrow 2H_2O$ external

Hydrolysis Reaction:

$Al^{3+} + H_2O \leftrightarrow AlOH^{2+} + H^+$ internal

pH determined by $[Al^{3+}]/[AlOH^{2+}]$ in this range

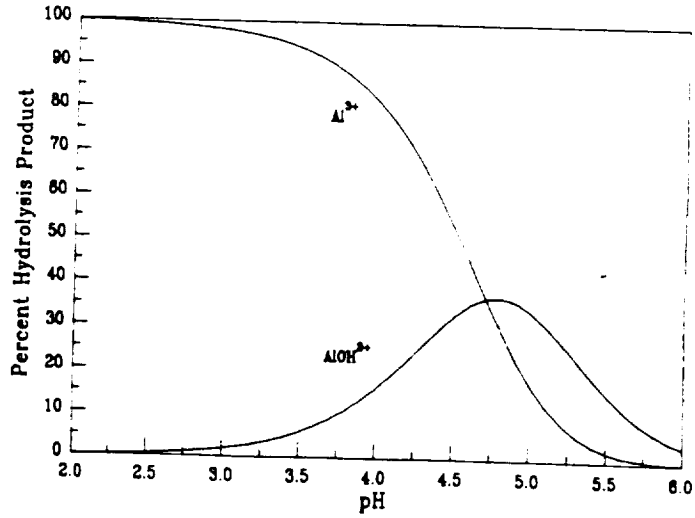

Results for Aluminum

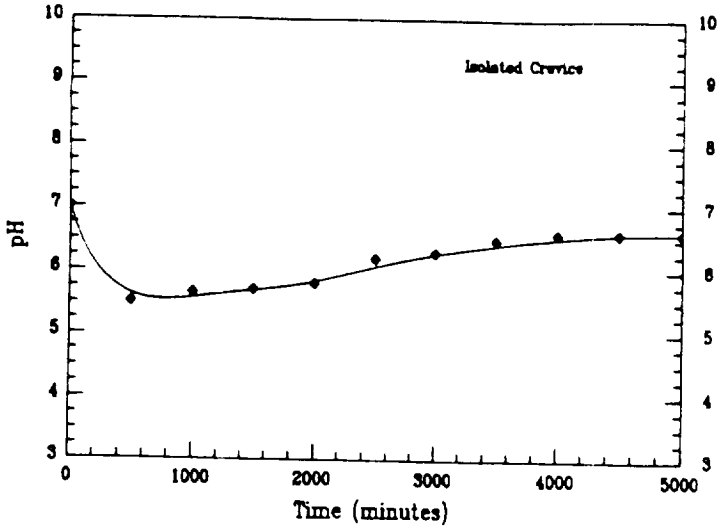

Electrochemical Reactions:

$Al \rightarrow Al^{3+} + 3e^-$ internal

$3H^+ + 3e^- \rightarrow 3/2H_2$ internal

dissolution of 1 Al consumes 3 H^+

Hydrolysis Reactions:

$Al^{3+} + H_2O \rightarrow AlOH^{2+} + H^+$ net loss of 2 H^+

$Al^{3+} + 2H_2O \rightarrow Al(OH)_2^+ + 2H^+$ net loss of 1 H^+

$Al^{3+} + 3H_2O \rightarrow Al(OH)_3 + 3H^+$ no net loss of H^+

$Al^{3+} + 4H_2O \leftarrow Al(OH)_4^- + 4H^+$ net gain of 1 H^+

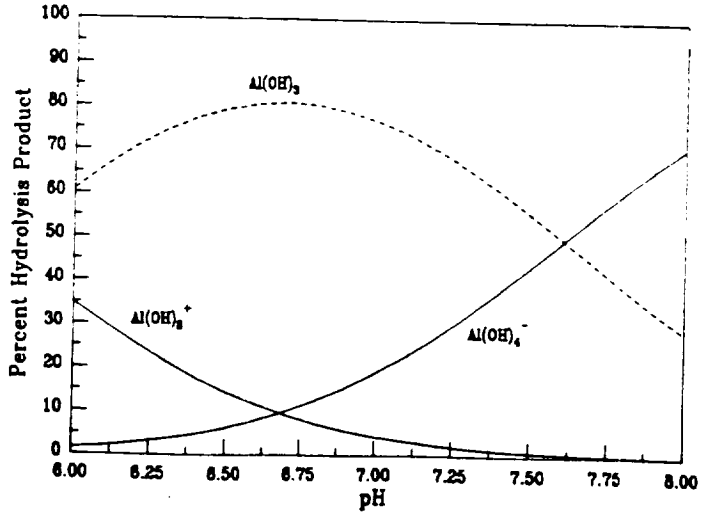

Results for SHT Al-3Li

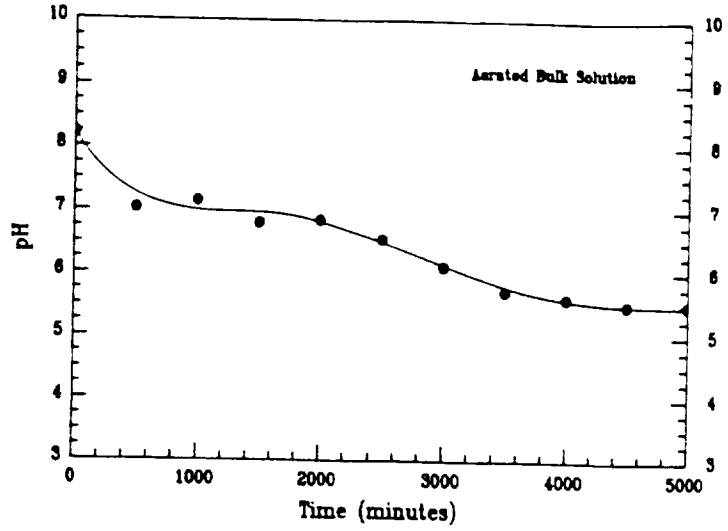

Electrochemical Reactions:

$Al \rightarrow Al^{3+} + 3e^-$ internal

$Li \rightarrow Li^+ + e^-$ internal

$O_2 + 4H^+ + 4e^- \rightarrow 2H_2O$ external

Hydrolysis Reactions:

$\leftrightarrow AlOH^{2+} + H^+$

$\leftrightarrow Al(OH)_2^+ + 2H^+$

$\leftrightarrow Al(OH)_3 + 3H^+$

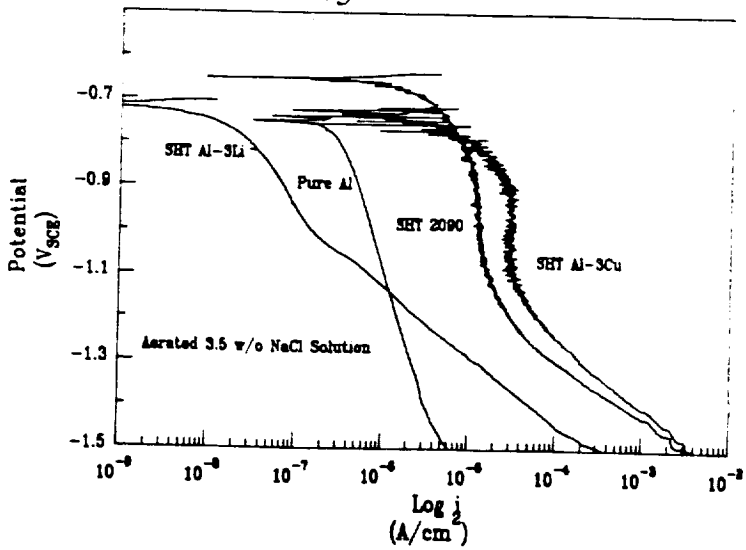

Reduction kinetics are slowed at the external cathode.

Results for SHT Al-3Li

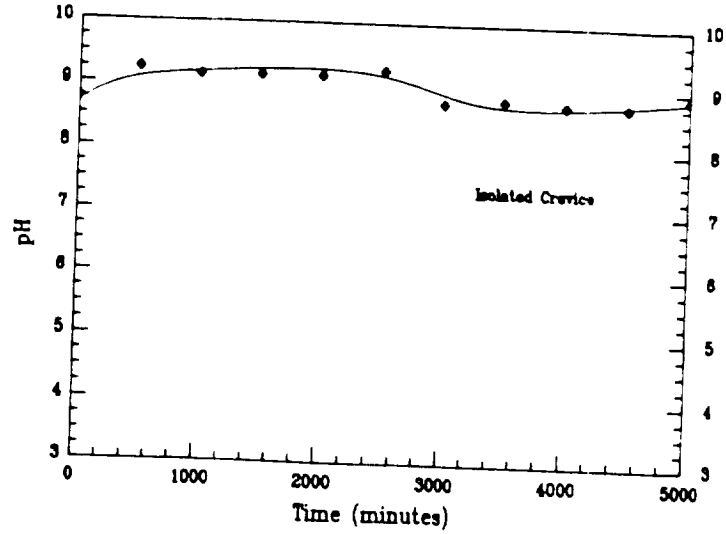

Electrochemical Reactions:

$Li \rightarrow Li^+ + e^-$ internal

$H^+ + e^- \rightarrow 1/2H_2$ internal

$H_2O + e^- \rightarrow H + OH^-$ internal

dissolution of 1 Li consumes 1 H^+

Hydrolysis Reactions:

$Li^+ + H_2O \leftrightarrow LiOH + H^+$ no net loss of H^+

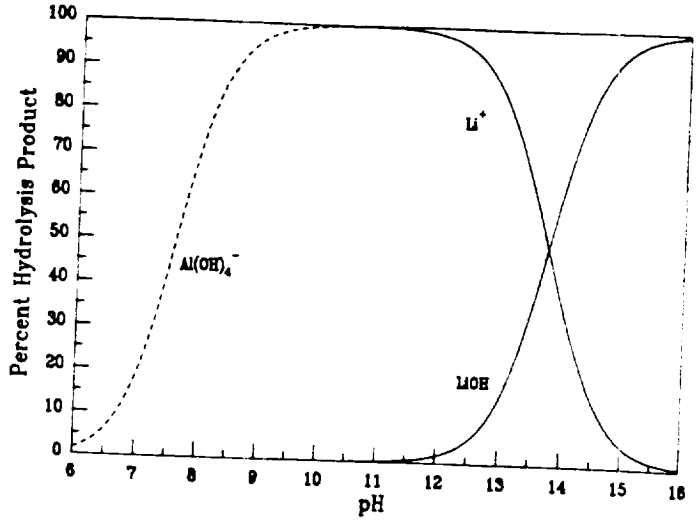

Results for SHT Al-3Cu

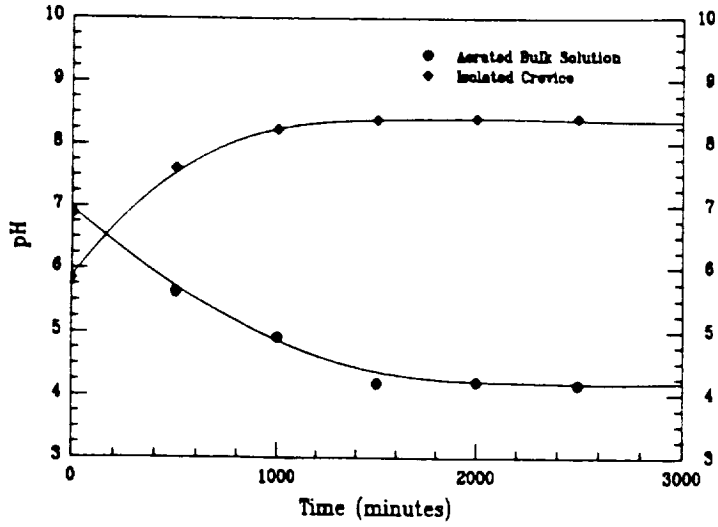

Aerated Bulk Solution

Consistent with $Al^{3+} + H_2O \leftrightarrow AlOH^{2+} + H^+$ equilibrium.

Isolated Crevice

Electrochemical Reactions:

$Cu \rightarrow Cu^{2+} + 2e^-$ internal

$2H^+ + 2e^- \rightarrow H_2$ internal

dissolution of 1 Cu atom form the alloy consumes 2 H^+.

Copper oxidation can not discharge H^+.

In RRDE experiments with Al_2Cu at potentials below $E_{R\ Cu/Cu^{2+}}$, copper deposits have been observed. (Mazurkiewicz and Piotrowski, 1983).

$[Cu^{2+}] > 10^{-9}$ M not detected in these crevices.

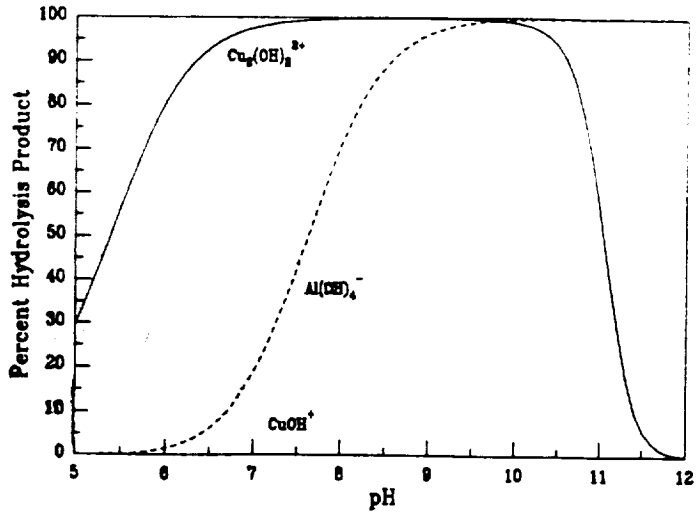

Results for SHT 2090

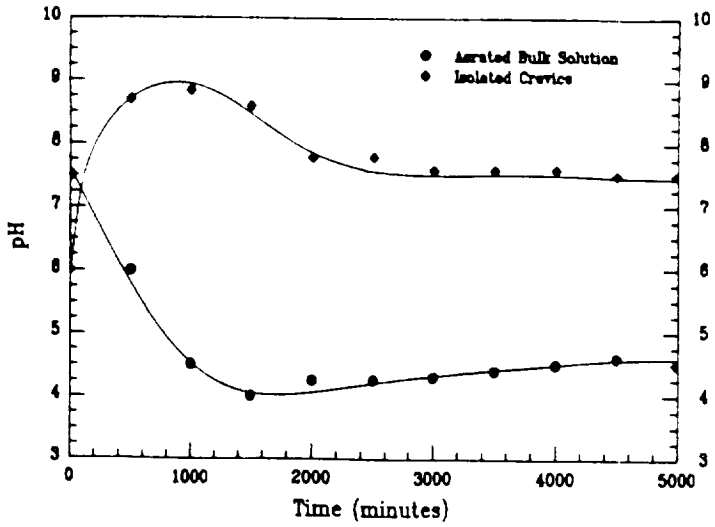

Aerated Bulk Solution

Consistent with $Al^{3+} + H_2O \leftrightarrow AlOH^{2+} + H^+$ equilibrium.

Isolated Crevice

$Li \rightarrow Li^+ + e^-$

$H^+ + e^- \rightarrow 1/2H_2$ assisted by elemental Cu on walls

$Li^+ + H_2O \leftrightarrow LiOH + H^+$

replaces H^+ and inhibits further pH increase.

Summary

* In aerated bulk solutions, crevice pH is consistent with:

$$Al^{3+} + H_2O \leftrightarrow AlOH^{2+} + H^+$$

dependent on reduction kinetics at the external cathode.

* $Al(OH)_2^+/Al(OH)_4^-$ system point defines the pH in pure Al, isolated crevices.

* $Li \rightarrow Li^+ + e^-$

  $H^+ + e^- \rightarrow 1/2H_2$ } gives an alkaline crevice

  $Li^+ + H_2O \leftrightarrow LiOH + H^+$ replaces H^+

* Elemental Cu on walls of crevices may assist in generating alkaline crevice solutions.